Atmospheric Environment 45 (2011) 4735–4744

Contents lists available at ScienceDirect

Atmospheric Environment

journal homepage: www.elsevier.com/locate/atmosenv

Impacts of HONO sources on the air quality in Beijing, Tianjin and Hebei Province of China

Ying Li [a,b], Junling An [a,*], Min Min [c], Wei Zhang [d], Feng Wang [a,b,e], Pinhua Xie [f]

[a] State Key Laboratory of Atmospheric Boundary Layer Physics and Atmospheric Chemistry (LAPC), Institute of Atmospheric Physics (IAP), Chinese Academy of Sciences, Beijing 100029, China
[b] Graduate University of Chinese Academy of Sciences, Beijing 100049, China
[c] Key Laboratory of Radiometric Calibration and Validation for Environmental Satellites, National Satellite Meteorological Center, China Meteorological Administration, Beijing 100081, China
[d] China Aviation Meteorological Center, Beijing 100122, China
[e] Anhui Public Meteorological Services Center, Hefei 230061, China
[f] Key Laboratory of Environment Optics and Technology, Anhui Institute of Optics and Fine Mechanics, Chinese Academy of Sciences, Hefei 230031, China

ARTICLE INFO

Article history:
Received 27 September 2010
Received in revised form
29 March 2011
Accepted 10 April 2011

Keywords:
Nitrous acid
Heterogeneous reaction
WRF–Chem
DOAS

ABSTRACT

Incorporated into the WRF–Chem model are the three HONO sources, i.e., the reaction of photo-excited NO_2 with water (NO_2^* chemistry), heterogeneous reactions on aerosol surfaces, and HONO emissions. Four case simulations were performed in Beijing, Tianjin, and Hebei Province (BTH region) in August of 2007. Results indicate that the NO_2^* chemistry yields 30–50 ppb enhancements in daily maximum 1-h surface O_3 concentrations in major cities and 3–10 ppb increases in monthly mean daily maximum 8-h surface O_3 concentrations in most areas of the BTH region. Heterogeneous reactions on aerosol surfaces lead to 5–20 ppb decreases in monthly mean NO_y concentrations in major cities over the BTH region. Heterogeneous reactions and HONO emissions are the largest, and the second largest contributor, accounting for ~59% and 26% of simulated HONO concentrations, respectively. The three HONO sources produce enhancements in monthly mean daytime (10:00–17:00) concentrations of NO_y (total reactive N-containing compounds), NO_2, HNO_3, HONO, and HO_x being −1 to −5 ppb, −1 to −3 ppb, −0.3 to 0.5 ppb, 20–50 ppt, and 1–3 ppt, respectively. Comparison with observations shows that inclusion of the three HONO sources into the WRF–Chem model can considerably improve HONO and O_3 simulations in the BTH region. For HONO the mean, the normal mean bias, the root mean square error, and the correlation coefficient is greatly improved from 0.04 to 0.56 ppb, from −97% to −39%, from 1.10 ppb to 0.51 ppb, and from −0.56 to 0.86, respectively, by comparison with the gas chemical mechanism only considered in the WRF–Chem model. This suggests that the three important HONO sources be included in air quality models, particularly in the areas with high emissions of NO_x and particulate matter.

1. Introduction

Nitrous acid (HONO) plays an important role in the photochemistry of the troposphere due to its photolysis by solar ultraviolet radiation into the hydroxyl radical (OH), which is one of the most significant oxidants in the atmosphere (Alicke et al., 2002). Recent observations indicated unexpected high HONO levels of up to several ppb in urban or rural areas in China (Su et al., 2008a,b; An et al., 2009; Qin et al., 2009) but the state-of-the-art WRF–Chem model (Grell et al., 2005) and CMAQ model (Byun and Schere, 2006) severely underestimated HONO observations due to only inclusion of gas-phase chemical mechanisms (Sarwar et al., 2008; An et al., 2011). Su et al. (2008b) proposed an unknown HONO source to explain observed high HONO levels during the daytime. Sarwar et al. (2008) added a heterogeneous reaction, a surface photolysis reaction, and HONO emissions to the CMAQ model and simulations still showed HONO underestimation by comparison with observations, particularly in the daytime. Li et al. (2008) suggested an additional HONO daytime source through the reaction of electronically excited nitrogen dioxide with water vapor,

$$NO_2 + h\upsilon(\lambda > 420\ \text{nm}) \rightarrow NO_2^* \quad \text{(R1)}$$

* Corresponding author. Tel.: +86 10 82080598; fax: +86 10 62024951.
E-mail address: anjl@mail.iap.ac.cn (J. An).

1352-2310/$ – see front matter © 2011 Elsevier Ltd. All rights reserved.
doi:10.1016/j.atmosenv.2011.04.086

Table 1
Options in the WRF–Chem model used in this study.

Options	WRF–Chem
Advection scheme	Runge–Kutta 3rd order
Cloud microphysics	Lin et al.
Long-wave radiation	RRTM
Short-wave radiation	Goddard
Surface layer	Monin–Obukhov
Land-surface model	Noah
Boundary layer scheme	YSU
Cumulus parameterization	New Grell scheme
Photolysis scheme	Madronich (1987)
Chemistry option	CBM-Z
Aerosol option	MOZAIC

$$NO_2^* + H_2O \rightarrow HONO + OH \quad (R2)$$

$$NO_2^* + M \rightarrow NO_2 + M \ (\text{where M is } N_2, O_2, \text{ or } H_2O) \quad (R3)$$

The reaction rate for Reaction R2 given by Li et al. (2008) is 1.7×10^{-13} cm^3 molecule^{-1} s^{-1}, which is an order of magnitude higher than that found by Crowley and Carl (1997). Although further experiments are needed to be done in order to reduce the uncertainty of the rate constant, the HONO increase due to Reaction R2 may potentially play a significant role in some industrialized areas with elevated emissions of NO_x (=NO + NO_2). Wennberg and Dabdub (2008) coupled the NO_2^* chemistry into an air quality model and found that ozone (O_3) simulations were increased by as much as 55 ppb in the South Coast Air Basin of California for a summer episode in 1987. Sarwar et al. (2009) did similar work but illustrated that simulated O_3 enhancements were considerably smaller than those reported by Wennberg and Dabdub (2008) due primarily to much lower emissions of NO_x and volatile organic compounds (VOCs) in 2001/2002 than those in 1987. Compared with those in California, current emissions of NO_x and particulate matter in Beijing, Tianjin, and Hebei Province (BTH region) are very high (Zhang et al., 2009), so contributions of the NO_2^* chemistry and heterogeneous reactions on aerosol surfaces to O_3, NO_y (=NO_x + HONO + HNO_3 + PAN + other reactive N-containing compounds), HONO, NO_x, HO_x (=OH + HO_2), and HNO_3 in the BTH region could be significant and will be quantified in this paper by using the WRF–Chem model, which couples the newly developed modules of the NO_2^* chemistry, heterogeneous reactions on aerosol surfaces, and HONO emissions.

2. Model description

2.1. WRF–Chem model

The model used in this study is the Weather Research and Forecasting/Chemistry (WRF–Chem) model version 3.2 (Grell et al., 2005; Fast et al., 2006). The WRF–Chem model has two components: a meteorological module and a chemistry module. Both components use the same mass and scalar preserving flux scheme, the same physics schemes for subgrid-scale transport, the same horizontal and vertical resolutions, and the same time step (Grell et al., 2005). More detailed description of the WRF–Chem model can be found on the websites http://ruc.noaa.gov/wrf/WG11/ and http://www.wrf-model.org. The parameterization schemes used in this study are listed in Table 1. For gas chemistry used is the CBM-Z, an updated lumped-structure gas-phase photochemical mechanism (Zaveri and Peters, 1999). Photolysis rates are calculated by the TUV scheme (Madronich, 1987). The chosen aerosol module is MOSAIC (Zaveri et al., 2005a,b, 2008; Fast et al., 2006) with an 8-size-bin representation.

Two nested domains shown in Fig. 1 are employed for WRF–Chem simulations. Domain 1, 2, and 3 contains 83×65, 58×55 and 55×55 grid cells, with horizontal resolutions of 81, 27, and 9 km, respectively. Domain 3 primarily covers Beijing, Tianjin, and Hebei Province (BTH region). Twenty-eight vertical model layers from the surface to 50 hPa are used with nonuniform thickness. The lowest model layer is ~28 m above the ground. Meteorological initial and boundary conditions are from NCEP $1^\circ \times 1^\circ$ reanalysis data, which are also used for nudging every 6 h. The chemical initial and boundary conditions are updated by the output of a global chemical transport model MOZART-4 (Emmons et al., 2010) every 6 h. The detailed description of mapping species concentrations from the MOZART to the WRF–Chem can be found on the website http://www.acd.ucar.edu/wrf-chem/. Anthropogenic emissions in 2006/2007 were from Zhang et al. (2009). Considered were monthly variations of the emissions of SO_2, NO_x, CO, VOCs, PM_{10}, $PM_{2.5}$, BC, and OC. NH_3 emissions were provided by Streets et al. (2003). Biogenic emissions were calculated based on suggestions of Guenther et al. (1993, 1994) and Simpson et al. (1995). Model

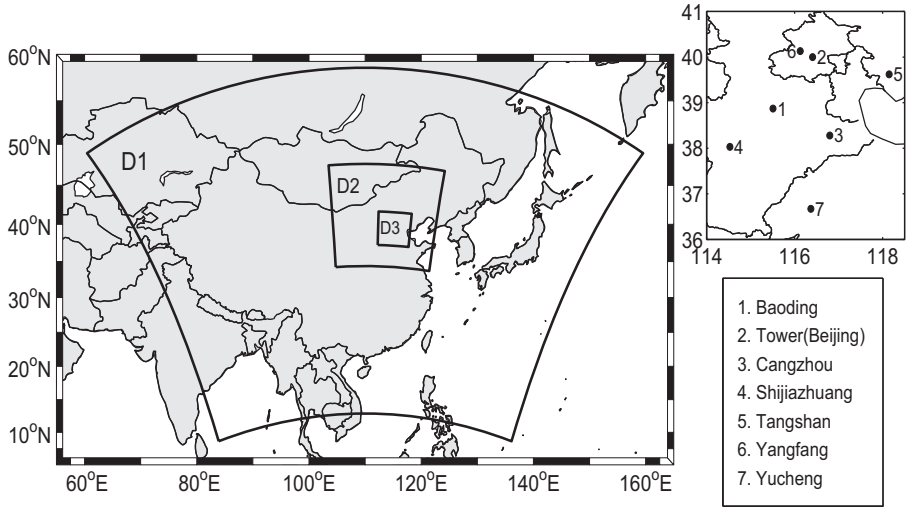

Fig. 1. Modeling domains used in this study and the seven measurement sites.

simulations were conducted from August 1 to 31 of 2007 with a spin-up period of 7 days (July 25–31).

Four case simulations, i.e., Case A, B, C and D, were performed to assess impacts of HONO sources on concentrations of O_3, NO_y, HONO, NO_x, HO_x, and HNO_3 in the BTH region. Case A is a reference, using the standard CBM-Z mechanism and the MOSAIC module. Case B includes Case A with Reactions R1–R3. Case C is the same as Case B besides inclusion of HONO emissions (see Section 2.2). Case D contains Case C with Reactions R4–R7 (see Section 2.2).

2.2. Parameterization of HONO sources

In addition to the homogeneous reaction of NO with OH, three sources of HONO are considered, i.e., the NO_2^* chemistry, heterogeneous reactions on aerosol surfaces, and HONO emissions, including secondary formation from NO_2 heterogeneous reaction with semivolatile organics. Specifically, the NO_2^* chemistry (Reactions 1–3) recommended by Li et al. (2008) is inserted to the CBM-Z mechanism. The rate of NO_2 photoexcitation is simplified as 3.5 times that of the photolysis of NO_2 because the former is 3–4 times higher than the latter (Ensberg et al., 2010). The rate constant for R2 is set as 9.1×10^{-14} cm^3 $molecule^{-1}$ s^{-1}, which is the mean value of 1.7×10^{-13} cm^3 $molecule^{-1}$ s^{-1} from Li et al. (2008) and 1.2×10^{-14} cm^3 $molecule^{-1}$ s^{-1} from Crowley and Carl (1997). The quenching rate constant for Reaction R3 is 2.7×10^{-11}, 3.0×10^{-11}, and 1.7×10^{-10} cm^3 $molecule^{-1}$ s^{-1} for N_2, O_2, and H_2O, respectively (Li et al., 2008).

For heterogeneous reactions on aerosol surfaces we follow Jacob (2000) recommendations,

$$HO_2 \rightarrow 0.5H_2O_2 \quad \gamma = 0.2 \tag{R4}$$

$$NO_3 \rightarrow HNO_3 \quad \gamma = 0.001 \tag{R5}$$

$$NO_2 \rightarrow 0.5HNO_3 + 0.5HONO \quad \gamma = 0.0001 \tag{R6}$$

$$N_2O_5 \rightarrow 2HNO_3 \quad \gamma = 0.1 \tag{R7}$$

The reactive uptake of HO_2, NO_3, NO_2, and N_2O_5 by aerosols is parameterized as follows (Jacob, 2000),

$$k = \left(\frac{a}{D_g} + \frac{4}{\nu\gamma}\right)^{-1} A_s \tag{1}$$

where k is the first-order rate constant; a is the particle radius (m); D_g denotes the gas-phase molecular diffusion coefficient, being 10^{-5} m^2 s^{-1} (Dentener and Crutzen, 1993); ν stands for the mean molecular speed (m s^{-1}); A_s is the aerosol surface area per unit volume of air, and γ denotes the uptake coefficient of reactive species. Considered aerosols are sulfate, nitrate, organic carbon, and black carbon. A lognormal number distribution is assumed for the considered aerosols to calculate A_s according to a different geometric mean radius and a standard deviation for each type of aerosol (Chin et al., 2002). Hygroscopic growth of the aerosols mentioned above is taken into account and listed in Table 2.

Table 2
Hygroscopic growth factors of r_e/r_{dry} at different relative humidity (RH). r_e is the cross section weighted effective radius at RH whereas r_{dry} is that when RH equals zero (Chin et al., 2002).

RH (%)	0	50	70	80	90	95	99
Sulfate	1	1.4	1.5	1.6	1.8	1.9	2.2
Nitrate	1	1.4	1.5	1.6	1.8	1.9	2.2
OC	1	1.2	1.4	1.5	1.6	1.8	2.2
BC	1	1.0	1.0	1.2	1.4	1.5	1.9

HONO emissions are estimated by using the HONO/NO_x emission ratio. Kurtenbacha et al. (2001) gave a HONO/NO_x ratio of 0.8% for high traffic density on an average working day. The value of 0.8% is adopted in other studies (Aumont et al., 2003; Sarwar et al., 2008). Gutzwiller et al. (2002) performed an experimental study and showed that a fraction of 2.3% of the NO_x emitted in diesel exhaust was heterogeneously converted to HONO. Assumed in this study is the HONO/NO_x emission ratio (ER) of 3.2% for diesel vehicles and that of 0.8% for gasoline vehicles. For all anthropogenic NO_x emissions the ER is calculated by $(3.2\% \times FD + 0.8\% \times (1 - FD)) \times FV$, where FD denotes the ratio of NO_x emissions from diesel vehicles to those from the total vehicles. FD is variable in different areas and its mean value is 62% in China (unpublished statistical data in 2006 from Chinese Research Academy of Environmental Sciences). FV stands for the ratio of NO_x emissions from the total vehicles to those from all anthropogenic sources. FV is a variable and its value can be found from China Statistical Yearbook 2007. For simplicity an averaged value of 1.08% is used for ER in this study.

3. Results and discussion

3.1. Impacts of HONO sources on O_3, NO_y, HONO, NO_x, HO_x, and HNO_3

Shown in Fig. 2 are the largest differences in simulated daily maximum 1-h O_3 between Cases B and A. Daily maximum 1-h O_3 concentrations are typically increased by 10–20 ppb in suburban areas, and 30–50 ppb enhancements are found in major cities, e.g., Beijing, Tianjin, and Shijiazhuang. The O_3 increases due to the NO_2^* chemistry in the BTH region are much larger than those of 1–13 ppb in U.S. shown by Sarwar et al. (2009). Monthly averaged daily maximum 8-h O_3 concentrations are increased within the range of 3–10 ppb in most areas of the BTH region, also higher than that of up to 2 ppb in U.S. (Sarwar et al., 2009). This indicates that

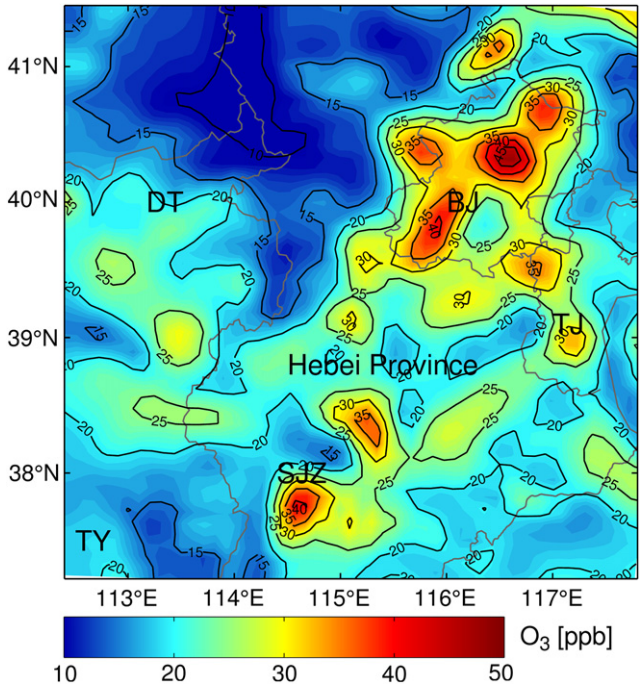

Fig. 2. Largest enhancements of daily maximum 1-h O_3 (ppb) in Beijing, Tianjin, and Hebei Province in August of 2007 due to the NO_2^* chemistry. BJ, TJ, DT, SJZ, and TY denotes Beijing, Tianjin, Datong, Shijiazhuang, and Taiyuan, respectively.

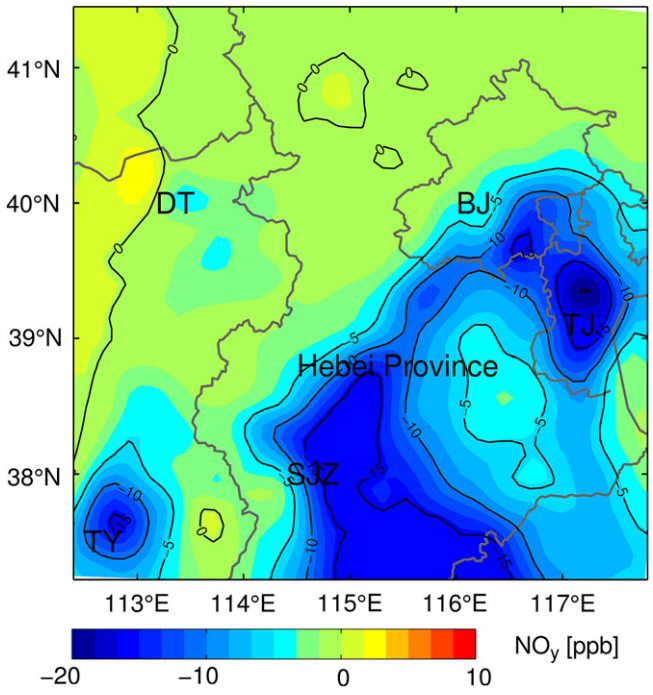

Fig. 3. Monthly mean NO_y concentration differences (ppb) near the surface in August of 2007 due to heterogeneous reactions on aerosol surfaces. BJ, TJ, DT, SJZ, and TY are the same as mentioned in Fig. 2.

the NO_2^* chemistry contributes much to O_3 formation in the BTH region, and confirms the significance of the NO_2^* chemistry in some industrialized regions with high emissions of NO_x as suggested by Sarwar et al. (2009). For HONO the NO_2^* chemistry causes hourly increases of 0.6–0.8 ppb in daytime (10:00–17:00) in major cities over the BTH region and the largest increase of 0.9 ppb located over the Bohai Bay. The result is similar to that of Sarwar et al. (2009).

High concentrations of particulate mater (PM) in Beijing, Tianjin, and Shijiazhuang lead to 5–20 ppb decreases in monthly mean NO_y concentrations near the surface when heterogeneous reactions are considered (Fig. 3). Comparatively, during the nighttime, the high relative humidity, low heights of the planetary boundary layer, and stable atmospheric conditions are favorable for increases in PM concentrations and PM hygroscopic growth rates and finally cause much more NO_y decreases in the nighttime than those in the daytime over the BTH region, where acid deposition could be aggravated as suggested by An et al. (2011).

Impacts of the three HONO sources on monthly mean concentration differences of HO_x, O_3, HONO, NO_x, NO_y and HNO_3 in the daytime (10:00–17:00) are shown in Fig. 4. HO_x concentrations are typically increased by 1–3 ppt, and the maximum enhancement is located in Beijing (Fig. 4a), where HO_x concentrations are nearly doubled. Enhanced HO_x concentrations can increase oxidation of NO to NO_2; subsequent photolysis of NO_2 yields more O_3 (Wennberg and Dabdub, 2008) as shown in Fig. 4b. That is why concentration difference distributions of O_3 are similar to those of HO_x (Comparing Fig. 4a and b). The maximum increase of 4 ppb is found in major cities in the BTH region, e.g., Beijing, Shijiazhuang, and Taiyuan. Averagely, HONO concentrations are enhanced by 20 ppt, with a maximum increase of 50 ppt located in Tianjin and Beijing (Fig. 4c). NO_2 concentrations are reduced by more than

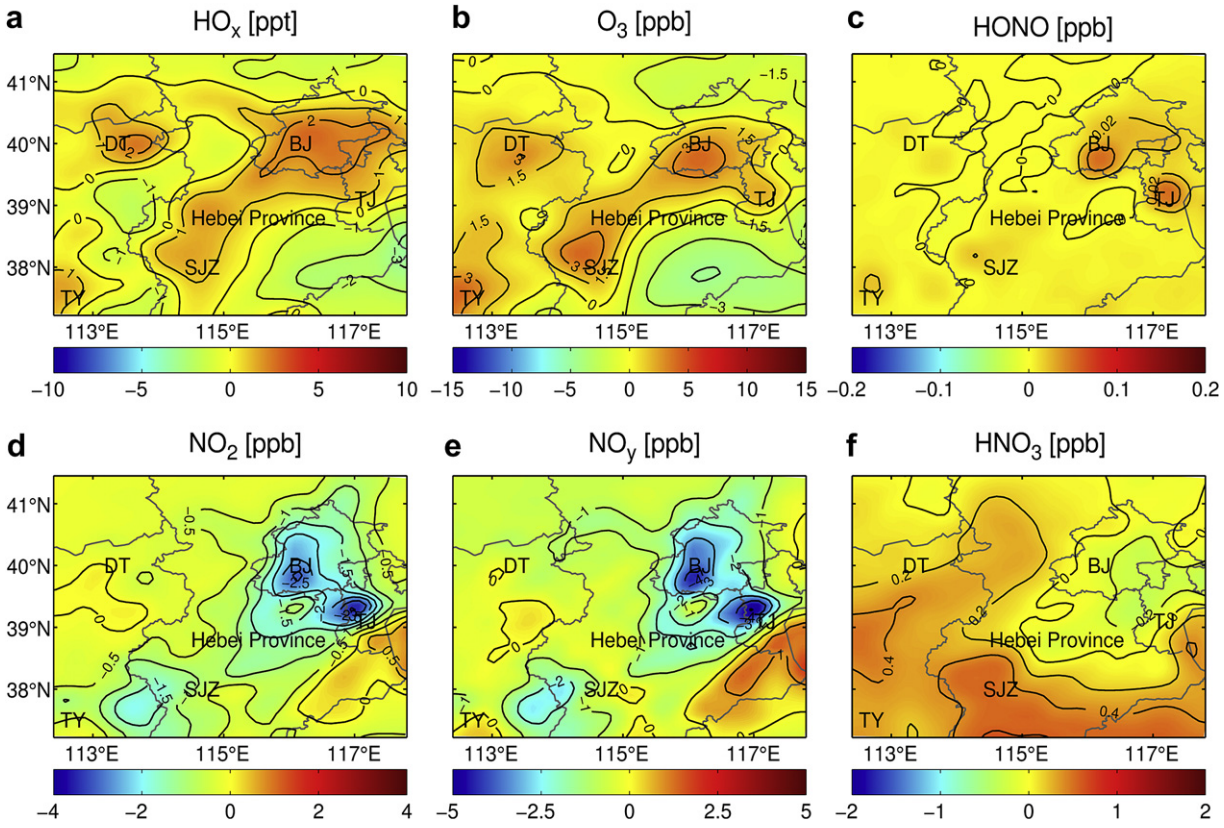

Fig. 4. Monthly mean concentration differences (ppb) near the surface from 10:00 to 17:00 in August of 2007 for the selected gases due to the three HONO sources in Beijing, Tianjin and Hebei Province. BJ, TJ, DT, SJZ, and TY are the same as mentioned in Fig. 2.

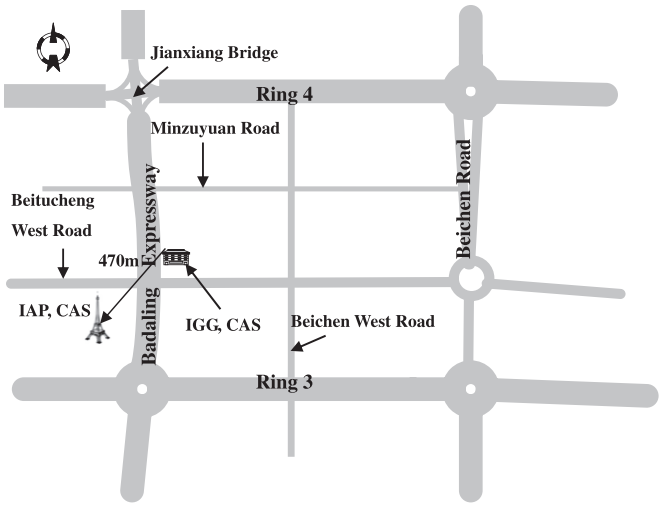

Fig. 5. Schematic map of the measurement site in Beijing. IAP, IGG, and CAS denotes Institute of Atmospheric Physics, Institute of Geology and Geophysics, and Chinese Academy of Sciences, respectively. The tower icon stands for the place where the 325 m Meteorological Tower is located.

3 ppb in Beijing and Tianjin (Fig. 4d) due to the increased oxidation rate of NO_2 to gaseous nitric acid (HNO_3) and heterogeneous reactions (e.g., Reaction R6). HONO and HNO_3 are scavenged more easily than NO_x, and result in NO_y decreases, with a maximum decrease of 5 ppb found in Tianjin (Fig. 4e). Changes in HNO_3 concentrations within a range of −0.3 and 0.5 ppb (Fig. 4f) are a combined result of HNO_3 increases due to heterogeneous reactions and HNO_3 decreases due to its dry and wet deposition.

3.2. Comparison of simulations and observations

3.2.1. Observed data used for model comparison

Differential Optical Absorption Spectroscopy (DOAS) measurements were conducted in Beijing from August 13 to 25, 2007 (Zhu et al., 2009). The DOAS system was sited on the roof of the office building of the Institute of Geology and Geophysics (IGG), Chinese Academy of Sciences (CAS). The retroreflector array was placed on the 15-m-high platform of the 325 m Meteorological Tower located at the Institute of Atmospheric Physics (IAP), where the traffic emissions were large (An et al., 2009). The fixed light path was 470 m (one way) across the Badaling expressway (Fig. 5). The DOAS system was described in detail by Zhu et al. (2009) and Qin et al. (2006). The specific detection limit is 0.41 ppb for HONO, 2.17 ppb for O_3, and 0.63 ppb for NO_2, respectively (Zhu et al., 2009). Surface concentrations of O_3, NO_x, and particulate matter ($PM_{2.5}$ and PM_{10}) were also simultaneously monitored at seven sites, including the 325 m Meteorological Tower site, across the BTH region, partially as Beijing Atmospheric Environmental Monitoring Action carried out by CAS. O_3 was measured with a Thermo Environmental Instrument (TEI) Model 49C analyzer, with a detection limit of 2 ppb (An et al., 2007). NO_x was measured by chemiluminescent gas analyzer (TEI Model 42C), with a detection limit of 0.05 ppb (An et al., 2007). The correlations between the DOAS system and O_3 and NO_2 analyzers were quite good, with the correlation coefficients being 0.97 for O_3 and 0.83 for NO_2. Mass concentrations of $PM_{2.5}$ and PM_{10} were measured with an RP1400a (Rupprecht & Patashnick, U.S.A.), with a detection limit of 1.5 μg m^{-3} (Zhang et al., 2006).

3.2.2. Comparison of simulated and observed HONO concentrations

For Case A simulated HONO concentrations are always substantially underestimated by comparison with observations in the period of August 13–25, 2007 (Fig. 6). The mean simulated HONO concentration is 0.04 ppb, ~25 times lower than the corresponding observed value. When the NO_2^* chemistry (R1–R3) is incorporated into the WRF–Chem model (Case B), daytime HONO concentrations are increased by ~0.03 ppb on average, and the maximum enhancement reaches 0.07 ppb at 9:00 (Fig. 6b). When HONO emissions are added to the WRF–Chem model (Case C), mean HONO simulations are enhanced to 0.21 ppb and nighttime HONO concentrations are considerably increased, ranging from 0.2 to 0.5 ppb, and reaching 0.43 ppb at sunrise. The normal mean bias (NMB) and the root mean square error (RMSE) are improved to −77% and 0.88 ppb, respectively (Table 3). When the three sources of HONO are added to the WRF–Chem model (Case D), simulations well follow HONO observations. The mean HONO

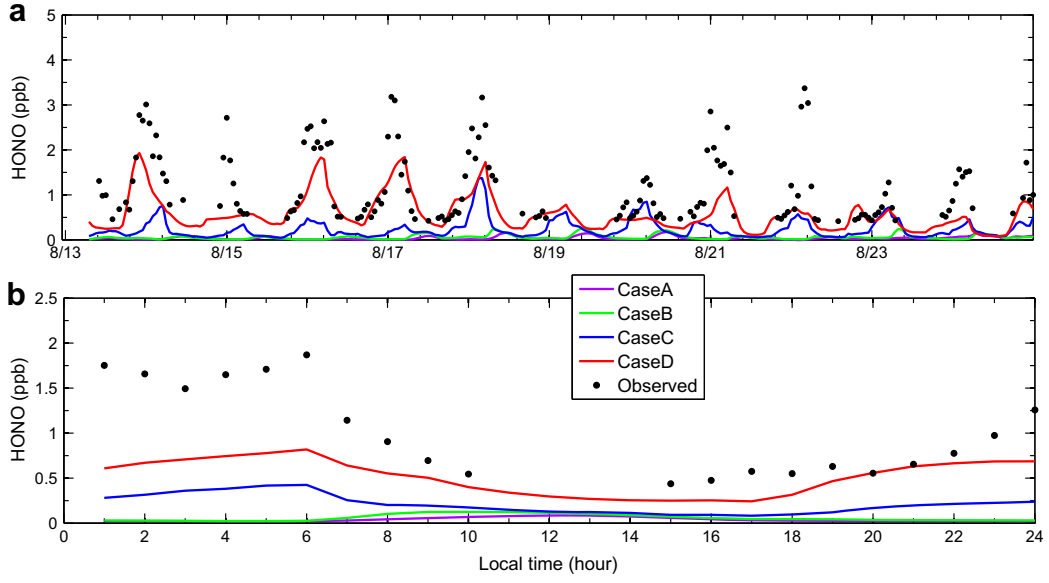

Fig. 6. Comparison of simulated (a) hourly mean and (b) diurnal-mean HONO concentrations with observations from DOAS.

Table 3
Model performance statistics for simulated diurnal-mean chemical species. HONO observations are from DOAS whereas the other observed data are from Chemiluminescence.

Cases	Mean observed (ppb)	Mean modeled (ppb)	MB (ppb)	NMB (%)	RMSE (ppb)	NME (%)	RC
A_{-HONO}	1.02	0.04	−0.98	−97	1.10	97	−0.56
B_{-HONO}	1.02	0.06	−0.97	−95	1.09	95	−0.51
C_{-HONO}	1.02	0.21	−0.78	−77	0.88	77	0.93
D_{-HONO}	1.02	0.56	−0.39	−39	0.51	40	0.86
A_{-O_3}	44.33	22.05	−22.27	−50	29.31	50	0.97
B_{-O_3}	44.33	25.17	−19.16	−43	25.64	43	0.95
C_{-O_3}	44.33	28.52	−15.80	−35	20.51	35	0.95
D_{-O_3}	44.33	34.16	−10.17	−22	15.09	23	0.98
A_{-NO_2}	19.90	14.80	−5.10	−26	6.09	26	0.77
B_{-NO_2}	19.90	15.68	−4.22	−21	5.36	21	0.81
C_{-NO_2}	19.90	16.39	−3.52	−17	4.98	21	0.88
D_{-NO_2}	19.90	15.20	−4.71	−24	6.06	25	0.85
A_{-NO}	4.48	7.93	3.45	77	3.73	77	0.94
B_{-NO}	4.48	4.94	0.46	10	1.70	32	0.92
C_{-NO}	4.48	4.08	−0.39	−9	2.38	41	0.80
D_{-NO}	4.48	3.57	−0.91	−20	1.36	21	0.98

simulation rises up to 0.56 ppb. The mean bias (MB), NMB, RMSE, the normal mean error (NME), and the correlation coefficient (RC) is improved to −0.39 ppb, −39%, 0.51 ppb, 40%, and 0.86, respectively (Table 3). However, simulated HONO concentrations for Case D still underestimate observations, especially in the nighttime. This may be related to unknown HONO sources. The uncertainty of the reaction rate for Reaction R2 also influences HONO simulations in the daytime. The low rate constant of 9.1×10^{-14} cm^3 $molecule^{-1}$ s^{-1} for Reaction R2 adopted in this study may lead to low HONO simulations at ~17:00 as shown in Fig. 6b. Li et al. (2008) demonstrates that the contribution from Reaction R2 will reduce when the solar zenith angle becomes low. Additionally, the WRF–Chem model frequently overestimates the HONO photolysis rate in the afternoon (Li et al., 2010), and Sarwar et al. (2008) also finds HONO underestimation in the afternoon. As discussed above, although there are some uncertainties in HONO simulations, the three HONO sources are important and can significantly improve HONO simulations when the three sources are contained in the WRF–Chem model.

Shown in Fig. 7 is the relative contribution of the HONO sources to simulated HONO concentrations. The heterogeneous reactions (R4–R7) are the largest contributor, accounting for 59% on average. The averaged contribution is close to 54% given by Sarwar et al. (2008). Sarwar et al. (2008) point out that the contribution of the heterogeneous reaction is up to 90% at night while that is much lower during the daytime. Contrastingly, our simulations indicate that the heterogeneous reaction contributes more than 40% all day. HONO emissions are the second largest contributor, accounting for 26% on average, with a maximum contribution of 51% at 5:00. On the contrary, Li et al. (2010) show that the most important HONO source is the secondary HONO formation from NO_2 reaction with semivolatile organics. This is mainly attributed to the chosen high $HONO/NO_x$ emission ratio of 2.3%, which needs to be further investigated. The averaged contribution of the homogeneous reaction is 9%, with the peak of 30% at 13:00. The contribution of the NO_2^* chemistry approaches the maximum of 12% at ~10:00.

Heterogeneous reactions on aerosol surfaces are significant for HONO formation and shown in Fig. 8 are simulated variations of $PM_{2.5}$, PM_{10}, total particle number (PN), and aerosol surface area per unit volume of air (SA) for Case D at the 325 m Meteorological Tower site during the period of August 13–25 of 2007. Simulated concentrations of $PM_{2.5}$ and PM_{10} reasonably follow observations (Fig. 8a, b). Observed PN and SA are not available in the simulation period. However, simulated PN is generally in the range of $(1.8 \pm 0.8) \times 10^4$ cm^{-3} in the Beijing urban area in summer of 2006 given by Yue et al. (2009), and simulated SA is roughly in the range of 227 μm^2 cm^{-3} on clear days to 3800 μm^2 cm^{-3} on smoky days in summer of Beijing shown by Xu et al. (2006). The minimum simulated SA is lower than observations because the considered aerosols for heterogeneous reactions shown in Fig. 8d only include sulfate, nitrate, organic carbon, and black carbon. By comparison with HONO simulations for Case D (Fig. 6a), we can see that simulated variations of SA are similar to those of HONO for Case D, indicating the importance of heterogeneous reactions in HONO simulations. In addition, aerosol hygroscopic growth has a significant impact on SA. Exclusion of aerosol hygroscopic growth

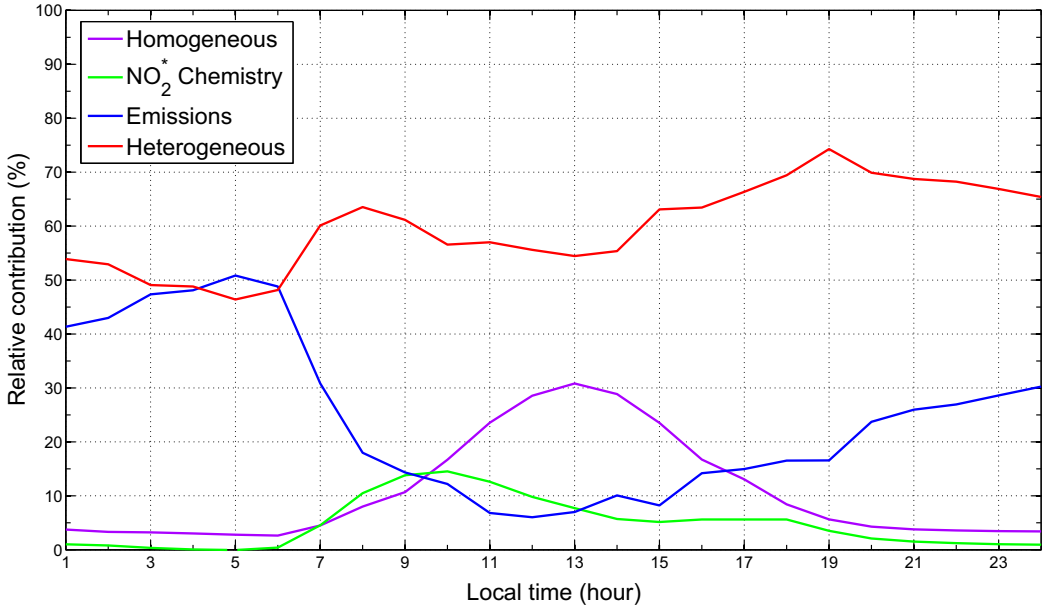

Fig. 7. Relative contributions of different sources to simulated HONO concentrations for Case D.

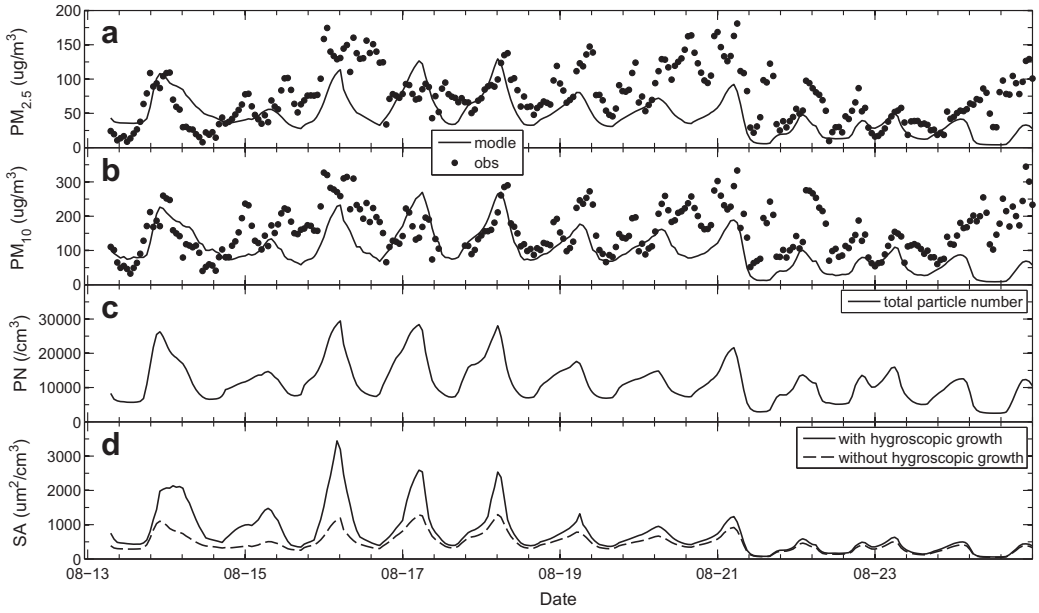

Fig. 8. Simulations of $PM_{2.5}$, PM_{10}, total particle number (PN) and aerosol surface area per unit volume of air (SA) and observations of $PM_{2.5}$ and PM_{10} at the 325 m Meteorological Tower in Beijing during the period of 13–25 August of 2007.

(Table 2) can lead to ~280 μm^2 cm^{-3} (38.3%) decreases in SA as shown in Fig. 8d.

3.2.3. *Comparison of simulated and observed O_3 and NO_2*

Daily O_3 peaks are significantly improved in most cases when the three HONO sources are included (Case D) although Cases A–D well follow observed O_3 diurnal variations (Fig. 9). Nice O_3 simulations for Case D are attributed to inclusion of the NO_2^* chemistry (Case B), HONO emissions (Case C), and heterogeneous reactions. This demonstrates the importance of the NO_2^* chemistry, heterogeneous reactions, and HONO emissions in the BTH region. Daily NO_2 simulations also show noticeable improvements at some sites, e.g., Shijiazhuang, in different period of time (Fig. 10), especially when the three HONO sources are contained (Case D). If

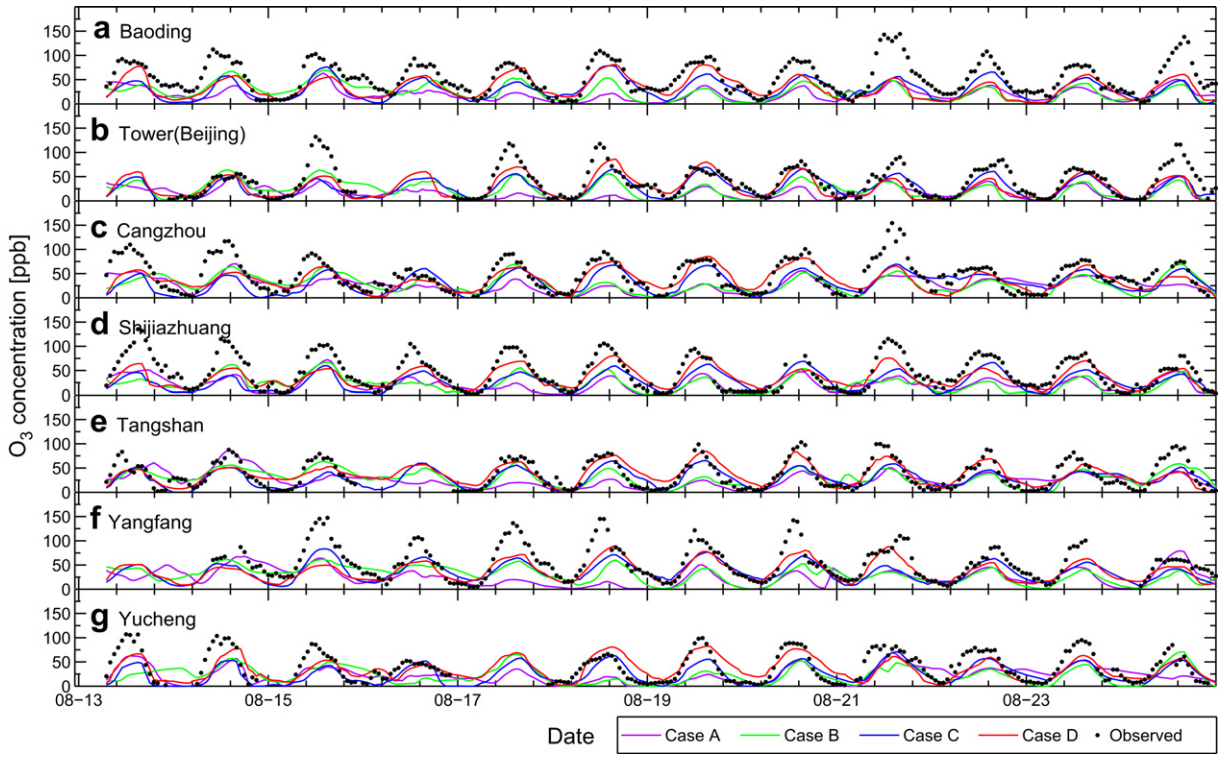

Fig. 9. Simulated and observed O_3 concentrations (ppb) at seven sites in Beijing, Tianjin, and Hebei Province during the period of 13–25 August of 2007. O_3 measurements are from Chemiluminescence.

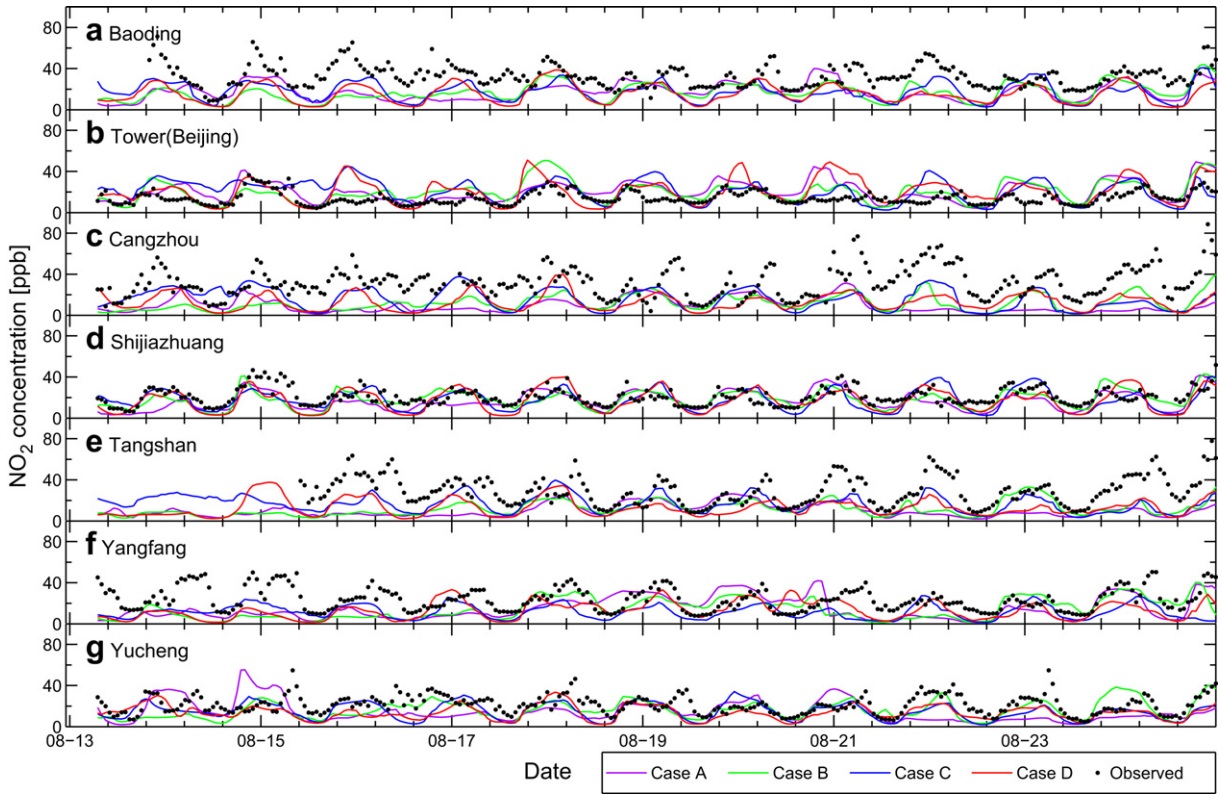

Fig. 10. Simulations and observations of NO_2 (ppb) at seven sites in Beijing, Tianjin, and Hebei Province during the period of 13–25 August of 2007. NO_2 measurements are from Chemiluminescence.

simulations and observations of O_3, NO_2, and NO at seven sites in the BTH region in August 13–25 of 2007 are averaged in one day, nighttime O_3 concentrations for Case D are fairly well simulated by comparison with observations (Fig. 11a). This may be attributed to that heterogeneous reactions could reduce ozone loss during the nighttime, particularly when SA is high (Kotamarthi et al., 2001). The maximum O_3 concentrations are substantially improved, from 38.7 ppb for Case A to 62.6 ppb for Case D (Fig. 11a). It should be emphasized that the increased HONO from the NO_2 heterogeneous reaction (R6) could accelerate NO → NO_2 conversion, leading to more O_3 formation. Xu et al. (2006) employ the air quality model CMAQ, including the four heterogeneous reactions, to simulate summer O_3 formation in Beijing, and show that the NO_2 and HO_2 heterogeneous reactions (R6 and R4) have significant impacts on O_3 formation, but effects of the NO_3 and N_2O_5 heterogeneous reactions (R5 and R7) on O_3 formation are quite small. They show that the NO_2 heterogeneous reaction (R6) could lead to the maximum O_3 increase of 67 ppb, which is much larger than the decreased value of 17 ppb due to the HO_2 heterogeneous reaction (R4). The combined result of the four heterogeneous reactions (R4–R7) produces a maximum O_3 increase of 50 ppb, being comparable to 58 ppb in our studies (Figures are not shown here). That is why O_3 simulations for Case D are higher than those for Case C during the daytime (Fig. 11a). Xu et al. (2006) also point out that the urban area of Beijing is a VOC-limited regime and HONO produced by heterogeneous reactions lead to an increase of new radicals, directly making up the scarcity of radicals in the urban area, accounting for O_3 increases.

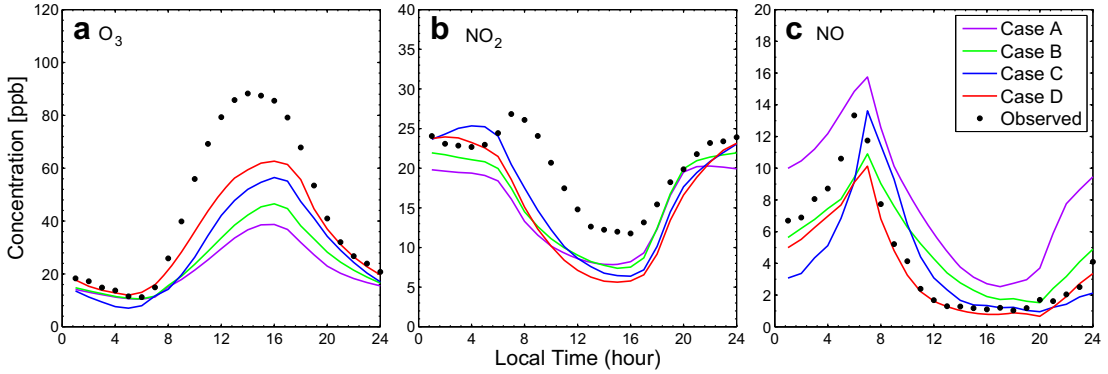

Fig. 11. Comparison of simulated diurnal-mean (a) O_3, (b) NO_2, and (c) NO concentrations with observations (ppb) averaged over the seven monitoring sites during the period of 13–25 August of 2007.

Observed NO_2 diurnal-mean variations show double peaks in the morning and at night (Fig. 11b). The WRF–Chem model reasonably simulates NO_2 diurnal variations for all cases (Fig. 11b). When the NO_2^* chemistry is incorporated into the WRF–Chem model, NO_2 concentrations are increased by 0.9 ppb on average compared with Case A, with the maximum enhancement of 2.1 ppb at midnight (Fig. 11b). NO_2 simulations for Case D are lower than those for Case C because of NO_2 heterogeneous reactions on aerosol surfaces. Case D improves NO_2 simulations during the nighttime but remains underestimation in the daytime (Fig. 11b). Observed NO diurnal-mean variations reach the peak of 13.3 ppb at 6:00 and show sharp decreases from 6:00 to 12:00 (Fig. 11c). When all HONO sources are included, NO simulations are nearly perfect by comparison with observations, particularly in the daytime.

4. Conclusions

Inserted into the state-of-the-art WRF–Chem model are the reaction of photo-excited NO_2 with water (NO_2^* chemistry), heterogeneous reactions on aerosol surfaces, and HONO emissions. Four case simulations were carried out in Beijing, Tianjin, and Hebei Province (BTH region) in the whole month of August of 2007. Results show that the NO_2^* chemistry, heterogeneous reactions, and emissions are key sources of HONO in the BTH region. The NO_2^* chemistry yields 30–50 ppb increases in daily maximum 1-h surface O_3 concentrations in major cities and 3–10 ppb enhancements in monthly averaged daily maximum 8-h O_3 concentrations near the surface in most areas of the BTH region. Heterogeneous reactions on aerosol surfaces cause 5–20 ppb decreases in monthly mean NO_y concentrations. Heterogeneous reactions are the largest contributor, accounting for ~59% of simulated HONO concentrations; HONO emissions are the second largest contributor, accounting for 26%. The three HONO sources lead to increases in monthly mean daytime (10:00–17:00) concentrations of NO_y (total reactive N-containing compounds), NO_2, HNO_3, HONO, and HO_x being −1 to −5 ppb, −1 to −3 ppb, −0.3 to 0.5 ppb, 20–50 ppt, and 1–3 ppt, respectively. Comparison with observations shows that inclusion of the three HONO sources in the WRF–Chem model can significantly improve HONO and O_3 simulations and have certain improvements in NO_2 simulations in the BTH region. For HONO the mean, the mean bias, the normal mean bias, the root mean square error, the normal mean error, and the correlation coefficient is significantly improved from 0.04 to 0.56 ppb, from −0.98 to −0.39 ppb, from −97% to −39%, from 1.10 ppb to 0.51 ppb, from 97% to 40%, and from −0.56 to 0.86, respectively, compared with exclusion of the three HONO sources in the WRF–Chem model. Simulations in the BTH region suggest that the NO_2^* chemistry, heterogeneous reactions, and HONO emissions should be contained in air quality models, particularly in the areas with elevated emissions of NO_x and particulate matter.

Acknowledgments

The research was partly supported by Knowledge Innovation Key Projects of Chinese Academy of Sciences (kzcx1-yw-06-04, KZCX2-YW-Q02-03, and kzcx1-yw-06-06) and the National Natural Science Foundation of China (Grant No. 40905055). Special thanks are given to Prof. Yuesi Wang for providing NO_2, O_3, $PM_{2.5}$ and PM_{10} observed data at seven sites in Beijing, Tianjin, and Hebei Province.

References

Alicke, B., Platt, U., Stutz, J., 2002. Impact of nitrous acid photolysis on the total hydroxyl radical budget during the Limitation of Oxidant Production/Pianura Padana Produzione di Ozono study in Milan. Journal of Geophysical Research 107 (D22), 8196. doi:10.1029/2000JD000075.

An, J., Wang, Y., Li, X., Sun, Y., Shen, S., Shi, L., 2007. Analysis of the relationship between NO, NO_2 and O_3 concentrations in Beijing. Environmental Science 28, 706–711 (in Chinese).

An, J., Zhang, W., Qu, Y., 2009. Impacts of a strong cold front on concentrations of HONO, HCHO, O_3, and NO_2 in the heavy traffic urban area of Beijing. Atmospheric Environment 43, 3454–3459.

An, J., Li, Y., Wang, F., Xie, P., 2011. Impacts of photoexcited NO_2 chemistry and heterogeneous reactions on concentrations of O_3 and NO_y in Beijing, Tianjin and Hebei Province of China. Air Quality/Book 1 (ISBN 978-953-307-1405-9). INTECH.

Aumont, B., Chervier, F., Laval, S., 2003. Contribution of HONO sources to the $NO_x/HO_x/O_3$ chemistry in the polluted boundary layer. Atmospheric Environment 37, 487–498.

Byun, D., Schere, K.L., 2006. Review of the governing equations, computational algorithms, and other components of the Models-3: Community Multiscale Air Quality (CMAQ) modeling system. Applied Mechanics Reviews 59, 51–77.

Chin, M., Ginoux, P., Kinne, S., Torres, O., Holben, B.N., Duncan, B.N., Martin, R.V., Logan, J.A., Higurashi, A., Nakajima, T., 2002. Tropospheric aerosol optical thickness from the GOCART model and comparisons with satellite and sun photometer measurements. Atmospheric Environment 43, 5731–5742.

Crowley, J.N., Carl, S.A., 1997. OH formation in the photoexcitation of NO_2 beyond the dissociation threshold in the presence of water vapor. Journal of Physics and Chemistry A 101, 4178–4184.

Dentener, F.J., Crutzen, P.J., 1993. Reaction of N_2O_5 on tropospheric aerosols' impact on the global distributions of NO_x, O_3, and OH. Journal of Geophysical Research 98, 7149–7163.

Emmons, L.K., Walters, S., Hess, P.G., Lamarque, J.-F., Pfister, G.G., Fillmore, D., Granier, C., Guenther, A., Kinnison, D., Laepple, T., Orlando, J., Tie, X., Tyndall, G., Wiedinmyer, C., Baughcum, S.L., Kloster, S., 2010. Description and evaluation of the model for ozone and related chemical tracers, version 4 (MOZART-4). Geoscientific Model Development 3, 43–67.

Ensberg, J.J., Carreras-Sospedra, M., Dabdub, D., 2010. Impacts of electronically photo-excited NO_2 on air pollution in the South Coast Air Basin of California. Atmospheric Chemistry and Physics 10, 1171–1181.

Fast Jr., J.D., Gustafson, W.I., Easter, R.C., Zaveri, R.A., Barnard, J.C., Chapman, E.G., Grell, G.A., Peckham, S.E., 2006. Evolution of ozone, particulates, and aerosol direct radiative forcing in the vicinity of Houston using a fully coupled meteorology-chemistry-aerosol model. Journal of Geophysical Research 111, D21305. doi:10.1029/2005JD006721.

Grell, G.A., Peckham, S.E., Schmitz, R., McKeen, S.A., Frost, G., Skamarock, W.C., Eder, B., 2005. Fully coupled "online" chemistry within the WRF model. Atmospheric Environment 39, 6957–6975.

Guenther, A.B., Zimmerman, P.R., Harley, P.C., Monson, R.K., Fall, R., 1993. Isoprene and monoterpene emission rate variability: model evaluations and sensitivity analyses. Journal of Geophysical Research 98, 12609–12617.

Guenther, A., Zimmerman, P., Wildermuth, M., 1994. Natural volatile organic compound emission rate estimates for US woodland landscapes. Atmospheric Environment 28, 1197–1210.

Gutzwiller, L., Arens, F., Baltensperger, U., Gaggeler, H.W., Ammann, M., 2002. Significance of semivolatile diesel exhaust organics for secondary HONO formation. Environmental Science and Technology 36, 677–682.

Jacob, D.J., 2000. Heterogeneous chemistry and tropospheric ozone. Atmospheric Environment 34, 2131–2159.

Kotamarthi, V.R., Gaffney, J.S., Marley, N.A., Doskey, P.V., 2001. Heterogeneous NO_x chemistry in the polluted PBL. Atmospheric Environment 35, 4489–4498.

Kurtenbacha, R., Beckera, K.H., Gomesa, J.A.G., Kleffmanna, J., Lorzera, J.C., Spittlera, M., Wiesena, P., Ackermannb, R., Geyerb, A., Plattb, U., 2001. Investigations of emissions and heterogeneous formation of HONO in a road traffic tunnel. Atmospheric Environment 35, 3385–3394.

Li, G., Lei, W., Zavala, M., Volkamer, R., Dusanter, S., Stevens, P., Molina, L.T., 2010. Impacts of HONO sources on the photochemistry in Mexico City during the MCMA-2006/MILAGO Campaign. Atmospheric Chemistry and Physics 10, 6551–6567.

Li, S., Matthews, J., Sinha, A., 2008. Atmospheric hydroxyl radical production from electronically excited NO_2 and H_2O. Science 319, 1657–1660.

Madronich, S., 1987. Photodissociation in the atmosphere. 1. Actinic flux and the effects of ground reflections and clouds. Journal of Geophysical Research 92, 9740–9752.

Qin, M., Xie, P., Liu, W., Li, A., Dou, K., Fang, W., Liu, J., Zhang, Y., 2006. Observation of atmospheric nitrous acid with DOAS in Beijing, China. Journal of Environmental Science 18, 69–75.

Qin, M., Xie, P., Su, H., Gu, J., Peng, F., Li, S., Zeng, L., Liu, J., Liu, W., Zhang, Y., 2009. An observational study of the HONO–NO_2 coupling at an urban site in Guangzhou City, South China. Atmospheric Environment 43, 5731–5742.

Sarwar, G., Roselle, S.J., Mathur, R., Appel, W., Dennis, R.L., Vogel, B., 2008. A comparison of CMAQ HONO predictions with observations from the Northeast Oxidant and Particle Study. Atmospheric Environment 42, 5760–5770.

Sarwar, G., Pinder, R.W., Appel, K.W., Mathur, R., Carlton, A.G., 2009. Examination of the impact of photoexcited NO_2 chemistry on regional air quality. Atmospheric Environment 43, 6383–6387.

Simpson, D., Guenther, A., Hewitt, C.N., Steinbrecher, R., 1995. Biogenic emissions in Europe. 1. Estimates and uncertainties. Journal of Geophysical Research 100, 22875–22890.

Streets, D.G., Bond, T.C., Carmichael, G.R., Fernandes, S.D., Fu, Q., He, D., Klimont, Z., Nelson, S.M., Tsai, N.Y., Wang, M.Q., Woo, J.-H., Yarber, K.F., 2003. An inventory of gaseous and primary aerosol emissions in Asia in the year 2000. Journal of Geophysical Research 108, D21. doi:10.1029/2002JD003093.

Su, H., Cheng, Y.F., Cheng, P., Zhang, Y.H., Dong, S., Zeng, L., Wang, X., Slanina, J., Shao, M., Wiedensohler, A., 2008a. Observation of nighttime nitrous acid (HONO) formation at a non-urban site during PRIDE-PRD2004 in China. Atmospheric Environment 42, 6219–6232.

Su, H., Cheng, Y.F., Shao, M., Gao, D.F., Yu, Z.Y., Zeng, L., Slanina, J., Zhang, Y., Wiedensohler, A., 2008b. Nitrous acid (HONO) and its daytime sources at a rural site during the 2004 PRIDE-PRD experiment in China. Journal of Geophysical Research 113, D14312. doi:10.1029/2007JD009060.

Wennberg, P.O., Dabdub, D., 2008. Rethinking ozone production. Science 319, 1624–1625.

Xu, J., Zhang, Y., Wang, W., 2006. Numerical study on the impacts of heterogeneous reactions on ozone formation in the Beijing Urban Area. Advances in Atmospheric Sciences 23, 605–614.

Yue, D., Hu, M., Wu, Z., Wang, Z., Guo, S., Wehner, B., Nowak, A., Achtert, P., Wiedensohler, A., Jung, J., Kim, Y.J., Liu, S., 2009. Characteristics of aerosol size distributions and new particle formation in the summer in Beijing. Journal of Geophysical Research 114, D00G12. doi:10.1029/2008JD010894.

Zaveri, R.A., Peters, L.K., 1999. A new lumped structure photochemical mechanism for large-scale applications. Journal of Geophysical Research 104, 30387–30415.

Zaveri, R.A., Easter, R.C., Peters, L.K., 2005a. A computationally efficient multicomponent equilibrium solver for aerosols (MESA). Journal of Geophysical Research 110, D24203. doi:10.1029/2004JD005618.

Zaveri, R.A., Easter, R.C., Wexler, A.S., 2005b. A new method for multi-component activity coefficients of electrolytes in aqueous atmospheric aerosols. Journal of Geophysical Research 110, D02201. doi:10.1029/2004JD005681.

Zaveri, R.A., Easter, R.C., Fast, J.D., Peters, L.K., 2008. Model for simulating aerosol interactions and chemistry (MOSAIC). Journal of Geophysical Research 113, D13204. doi:10.1029/2007JD008782.

Zhang, K., Wang, Y., Wen, T., Hu, B., Liu, G., Yousef, M., 2006. Studies on water soluble salts in PM_{10} during the heavy pollution process in Beijing. China Environmental Science 4, 385–389 (in Chinese).

Zhang, Q., Streets, D.G., Carmichael, G.R., He, K.B., Huo, H., Kannari, A., Klimont, Z., Park, I.S., Reddy, S., Fu, J.S., Chen, D., Duan, L., 2009. Asian emissions in 2006 for the NASA INTEX-B mission. Atmospheric Chemistry and Physics 9, 5131–5153.

Zhu, Y., Liu, W., Xie, P., Dou, K., Liu, S., Si, F., Li, S., Qin, M., 2009. Observational study of atmospheric HONO in summer of Beijing. Environmental Science 30, 1567–1573. in Chinese.